Multiphasic Effects of Cholesterol on Influenza Fusion Kinetics Reflect Multiple Mechanistic Roles

Marta K. Domanska,[†‡] Dominik Wrona,[†‡] and Peter M. Kasson[†‡*]
[†]Department of Molecular Physiology and Biological Physics and [‡]Department of Biomedical Engineering, University of Virginia, Charlottesville, Virginia

ABSTRACT The envelope lipid composition of influenza virus differs from that of the cellular plasma membrane from which it buds. Viruses also appear to fuse preferentially to specific membrane compartments, suggesting that the lipid environment may influence permissiveness for fusion. Here, we investigated the influence of the membrane environment on fusion, focusing on cholesterol composition. Strikingly, manipulating cholesterol levels in the viral membrane had different effects on fusion kinetics compared with analogous changes to the target membrane. Increasing cholesterol content in target vesicles increased lipid- and contents-mixing rates. Moderate cholesterol depletion from the viral membrane sped fusion rates, whereas severe depletion slowed the process. The pleiotropic effects of cholesterol include alterations in both membrane-bending moduli and lateral organization. Because influenza virions have demonstrated cholesterol-dependent lateral organization, to separate these effects, we deliberately selected a target vesicle composition that does not support lateral heterogeneity. We therefore postulate that the monotonic response of fusion kinetics to target membrane cholesterol reflects bending and curvature effects, whereas the multiphasic response to viral cholesterol levels reflects the combined effects of lateral organization and material properties.

INTRODUCTION

Membrane fusion is a crucial step in cell entry by enveloped viruses. In influenza virus, endosomal acidification causes rearrangement of the coat protein hemagglutinin, leading to exposure of fusion peptides that insert into the endosomal membranes and drive fusion (1,2). This is a dynamic process, and fusion intermediates are often studied by monitoring lipid and contents exchange between fusion partners (3). Mutagenesis studies have identified changes to the membrane-inserted fusion peptides that block fusion altogether or permit lipid exchange but not contents exchange (4–6). This can be interpreted to indicate at least two free-energy barriers to influenza fusion: one preceding lipid exchange and one after lipid but before contents exchange.

In addition to viral proteins, the lipid environment of both the viral envelope and the host cell can greatly influence the fusion process. Circumstantial evidence for this has long existed, as viral infection alters lipid synthesis pathways (7) and mature virus differs in lipid composition from either the membrane whence it came or uninfected cells (8). Cholesterol in particular is enriched in influenza virus (9). Cholesterol is of special interest because it can stabilize curved negatively membrane structures (10,11), can control lateral membrane organization (12,13), and is readily manipulable (unlike many lipid species, cholesterol can be easily added to or extracted from intact membranes). Cholesterol's effects on membrane fusion have been extensively studied, and cholesterol has been shown to be necessary for efficient neuronal exocytosis and enveloped viral entry (14–18).

To further probe the effects of cholesterol on influenza viral fusion, we studied how changes to viral or target membrane cholesterol affect fusion kinetics. Here, we report the use of fluorescence dequenching to measure fusion kinetics between live influenza virus and manipulable model membranes as a function of cholesterol content. Viral envelopes contain a complex lipid mixture; therefore, to separate the potential effects of cholesterol on lateral organization and curvature, we either extracted cholesterol from the native viral envelope or constructed simple target liposomes with varying amounts of cholesterol. We chose to use a target liposomal composition that does not support liquid-liquid phase coexistence.

MATERIALS AND METHODS

We used liposomes composed of 1-palmitoyl-2-oleoyl-sn-glycero-3-phosphocholine (POPC)/palmitoyloleoylphosphatidylethanolamine (POPE)/cholesterol (Chol)/NBD-dioleyl phosphatidylethanolamine (NBD-DOPE)/Rhodamine-DOPE extruded at 100 nm with aminonaphthalene-trisulfonic acid (ANTS)/p-xylene-bis-pyridinium bromide (DPX) complex encapsulated to monitor lipid and contents mixing simultaneously. Experiments were performed with excess DPX in the fusion buffer to suppress fluorescence signal from leakage and primarily measure contents mixing. We also performed controls without DPX in the buffer to assess leakiness during fusion. The resulting contents-release data (mixing + leakage) produced curve shapes that were indistinguishable from those obtained with mixing alone, indicating an absence of detectable leakage preceding fusion (Fig. 1). Additionally, solution measurements of ANTS fluorescence showed that the ANTS/DPX ratio present after total contents leakage was sufficient to quench >90% of ANTS fluorescence (Fig. S1 in the Supporting Material). Additional controls measuring dequenching of encapsulated ANTS alone with and without DPX in the fusion buffer suggested that minor leakage did occur, but that >90% of the signal in

Submitted February 11, 2013, and accepted for publication August 6, 2013.
*Correspondence: kasson@virginia.edu
Editor: Axel Brunger.

0006-3495/13/09/1383/5 $2.00
http://dx.doi.org/10.1016/j.bpj.2013.08.003

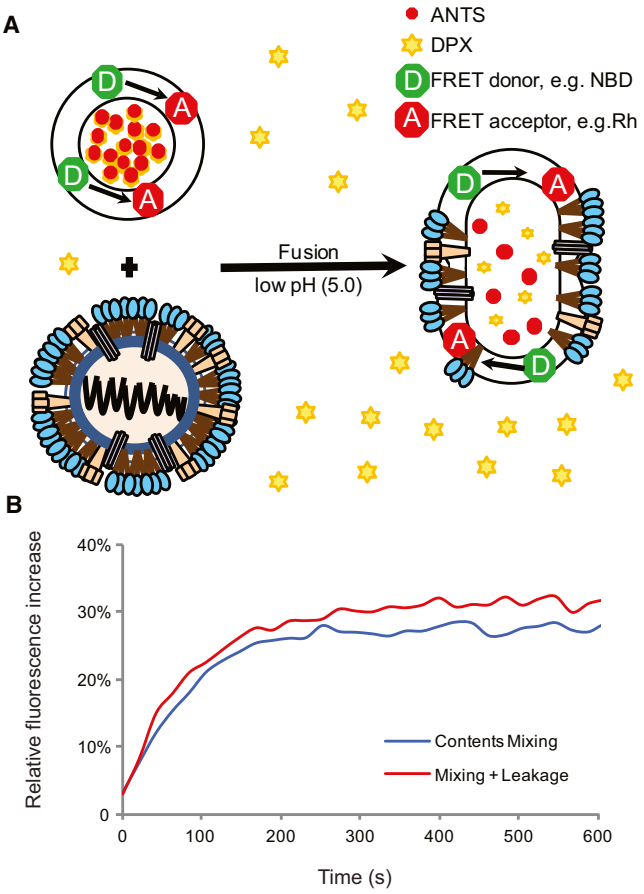

FIGURE 1 (*A*) Schema of the fusion assay. Fusion of influenza virus with labeled liposomes is monitored via fluorescence dequenching of lipidic and solution-phase dyes. Lipid mixing causes dilution of the NBD-DOPE and Rh-DOPE FRET pair, and thus an increase in NBD fluorescence. Contents mixing causes dilution of the ANTS/DPX complex and an increase in ANTS fluorescence. Additional DPX is present in the external buffer to quench free ANTS and differentiate mixing from leakage. (*B*) Representative traces with and without excess DPX in the external buffer.

fusion experiments with encapsulated ANTS/DPX was due to mixing (see Supporting Material).

Influenza virus

Egg-grown influenza virus X:31 (H3N2 A/Aichi/68) was purchased from Charles River Laboratories (Wilmington, MA). Cholesterol was extracted via incubation with 0, 10, 20, or 50 mM methyl-β-cyclodextrin (MβCD) at 37°C for 30 min. Virus was then reisolated from cyclodextrin-cholesterol complexes via centrifugation at 4°C, 14,000 rpm for 40 min, and then resuspended in buffer (10 mM phosphate/90 mM citrate/150 mM NaCl, pH 7.4).

Target liposomes

Large unilamellar vesicles (LUVs) composed of 30 mol % POPE, 1.5 mol % NBD-DOPE, 1.5 mol % Rh-DOPE, 10–40 mol % Chol (as specified), and the remaining 30–67 mol % POPC were extruded at 100 nm with ANTS/DPX contents dye encapsulated (internal concentration: 12.5 mM ANTS/45 mM DPX) and isolated by size-exclusion chromatography. Further details are given in the Supporting Material.

Fusion assay

Virus-liposome fusion was monitored via lipid and contents mixing, and assayed by fluorescence dequenching of the lipidic fluorescence resonance energy transfer (FRET) pair NBD/Rh and dissociation and dequenching of the soluble ANTS/DPX complex. Virus (standardized at 60 μg of viral protein) was mixed with target liposomes (0.2 mM total lipid), adjusted to a final buffer concentration of 30 mM DPX, and incubated for 30 min at 4°C. The reaction mixture was then warmed and equilibrated at 37°C over 15 min. Fusion was triggered by acidification to pH 5.0 using 2 mM citric acid, and fluorescence was monitored in a fluorescence plate reader. Excitation and emission wavelengths were set at 460 nm/538 nm (with a 530 nm cutoff filter) and 360 nm/530 nm (with a 515 nm cutoff filter) for NBD/Rh and ANTS/DPX, respectively. Lipid mixing values were normalized as follows: $I_{norm} = (I_{obs} - I_0) / (I_{max} - I_0)$, where I_0 is the fluorescence reading before acidification and I_{max} is the fluorescence reading after addition of Triton X-100 to a final concentration of 1%. Contents-mixing values were reported only as the relative increase in fluorescence over baseline: $I_{rel} = I_{obs} / I_0 - 1$. Fusion rates were determined via fitting to a single-exponential equation with a phase-shift parameter to allow for an experimental time lag between acidification and $t = 0$ time of fluorescence measurement. This yielded the following fit equation: $I_{norm}(t) = a * (1 - \exp(-b * (t + t_0)))$. Lipid dye transfer was observed only under conditions of fusion (Fig. S2), and contents dequenching was almost completely

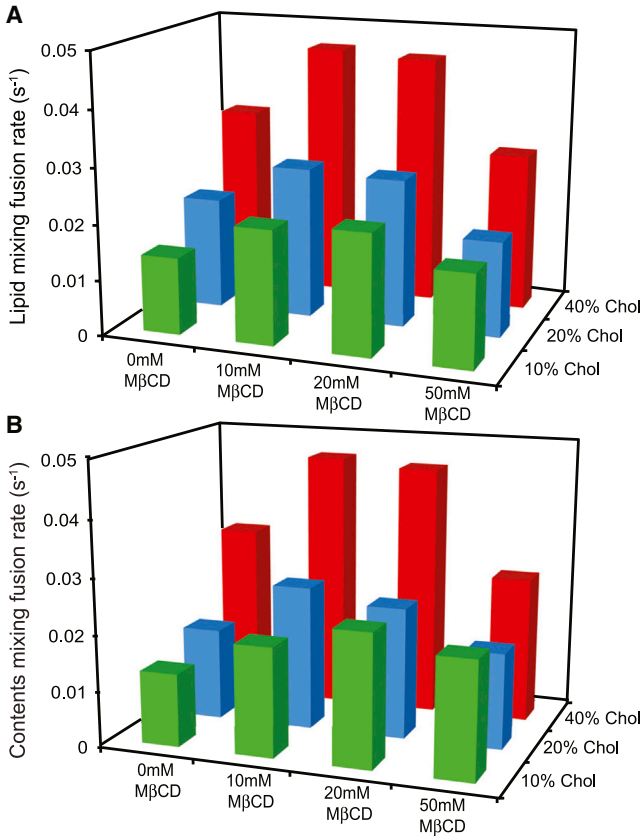

FIGURE 2 Lipid- and contents-mixing rates at different cholesterol compositions. (*A* and *B*) Rates of lipid mixing (*A*) and contents mixing (*B*) were determined via single-exponential fits to fluorescence dequenching traces. Mixing rates show a consistent increase with increasing mole fraction cholesterol in target vesicles. A biphasic response is observed with progressive cholesterol extraction from the virus. Each bar represents the median of five to 13 measurements. These trends can be visualized more clearly in Figure 3.

attributable to mixing, as measured by fluorescence of isolated fusion products (Table S1). Further details and dequenching controls are reported in the Supporting Material.

RESULTS AND DISCUSSION

To test how fusion kinetics change with target membrane composition, we varied the mole fraction cholesterol in target liposomes from 10 to 40 mol %. Fig. 2 *A* summarizes the lipid-mixing rates for our virus-liposome fusion experiments; normalized fusion rates are plotted as a function of liposomal cholesterol content in Fig. 3 *A*. Under all viral conditions tested, increasing liposomal cholesterol increased the fusion rates. We observed a nearly identical effect on contents mixing (Figs. 2 *B* and 3 *B*). Lipid-mixing rates of virus that was not treated with methyl-β-cyclodextrin increased 2.4-fold from 10 to 40 mol % liposomal cholesterol (0.014 s^{-1} to 0.033 s^{-1}). Similarly, the contents-mixing rate increased 2.3-fold (0.013 s^{-1} to 0.031 s^{-1}). Similar increases were observed at all viral cholesterol levels, indicating that increasing the cholesterol content of target membranes robustly speeds fusion independently of the viral membrane composition. Furthermore, we observed similar trends whether we held the mole fraction POPE in target vesicles constant at 30% or held the POPC/POPE molar ratio constant at 2:1 (Fig. S3).

According to previous reports (9) and assays we have performed on X:31 virus, influenza virus contains cholesterol/phospholipid in a ~1:1 ratio. Therefore, we manipulated the viral cholesterol composition via extraction with methyl-β-cyclodextrin (MβCD) rather than by supplementation. We verified the efficiency of extraction using a previously reported enzymatic assay for cholesterol content (18) and found a dose-dependent drop in cholesterol, with 75% depletion for 10 mM MβCD and nearly 90% depletion for 50 mM MβCD (Fig. 4). Normalized fusion rates are plotted as a function of MβCD dose in Fig. 3, *C* and *D*. In contrast to the monotonic effect of liposomal cholesterol, cholesterol extraction from the viral envelope yielded a biphasic response: fusion rates increased from 0 to 10 mM MβCD and then slowed down at 50 mM MβCD. For 20 mol % cholesterol vesicles, the lipid-mixing fusion rate increased from 0.02 s^{-1} without MβCD to 0.027 s^{-1} when virus was treated with 10 and 20 mM MβCD. Further extraction from the virion reduced the fusion rate to 0.017 s^{-1} at 50 mM MβCD. Similar trends occurred at 10 and 40 mol % cholesterol in the target vesicles (Figs. 2 and 3) and for lipid mixing as well as contents mixing. Importantly, the extent of both lipid and contents mixing decreased steadily with progressive extraction of cholesterol (Fig. S4). It is the kinetics of the fusion process, rather than the efficiency, that showed a biphasic response.

Cyclodextrin can be used as a bidirectional cholesterol carrier, so to test the reversibility of cholesterol removal from influenza virions, we performed replenishment experiments by adding cholesterol back using a cholesterol-MβCD carrier complex as previously described (19). We observed full reversibility of cholesterol extraction, assayed via both cholesterol content and fusion efficiency, at MβCD concentrations as high as 20 mM. At 50 mM MβCD, cholesterol content and fusion efficiency were both partially restored (Fig. 4), indicating a loss of some viable virus. Hemagglutination titers performed on virus treated with 0 mM and 50 mM MβCD yielded measurements of

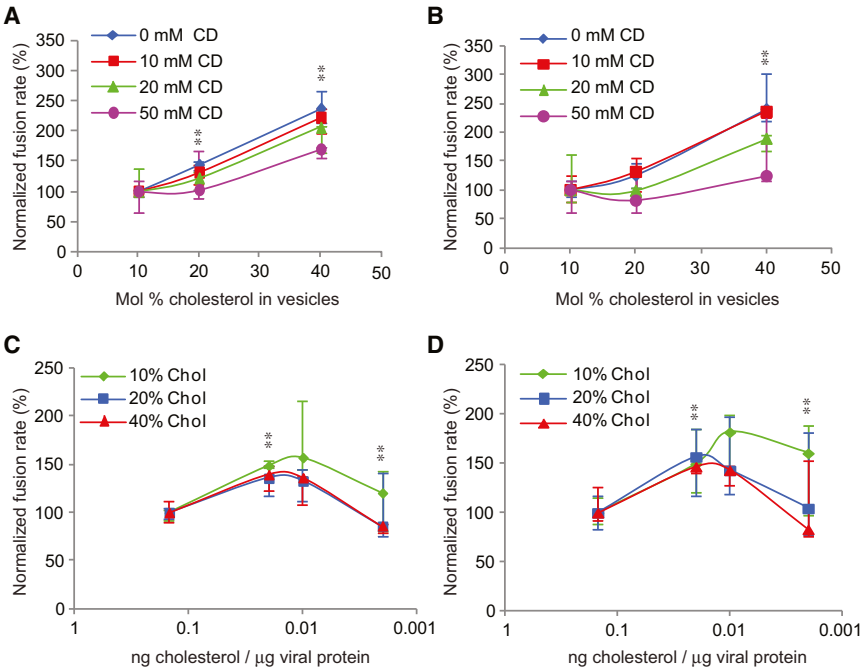

FIGURE 3 Response of fusion kinetics to altered cholesterol levels in influenza virions or target vesicles. Normalized fusion rates are plotted to visualize trends more clearly; these correspond to the unnormalized rates plotted in Figure 2. (*A* and *B*) Rates of lipid (*A*) and contents (*B*) mixing are plotted as a function of mol % cholesterol in target vesicles. (*C* and *D*) Rates of lipid (*C*) and contents (*D*) mixing are plotted as a function of the cholesterol/viral protein ratio after cyclodextrin treatment. Significance was assessed via the Kolmogorov-Smirnov test with a Bonferroni multiple-hypothesis correction; ** denotes a significant change from both the baseline and the prior condition, $p < 0.02$. Error bars are plotted as interquartile ranges. Trend lines are placed as visual guides.

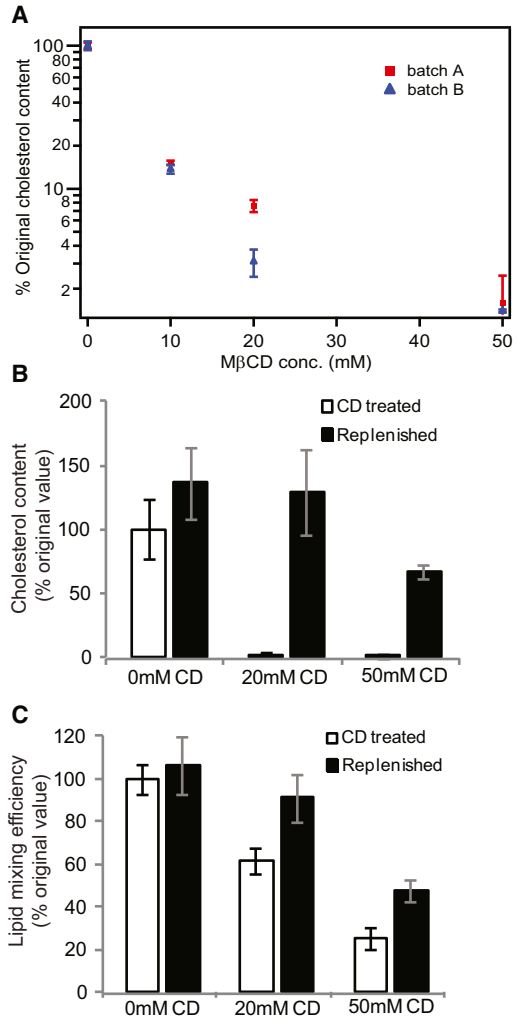

FIGURE 4 Cholesterol depletion from and replenishment of influenza virions. (*A*) Relative cholesterol depletion from X:31 influenza virions as a function of MβCD treatment. Error bars are plotted as the SD over four independent measurements per condition. Initial cholesterol levels were measured at 0.15 $\pm$ 0.0043 and 0.22 $\pm$ 0.0153 ng cholesterol per microgram of viral protein for batches A and B, respectively. (*B*) Results of cholesterol replenishment experiments after extraction with 0, 20, or 50 mM MβCD. (*C*) Results of lipid-mixing efficiency experiments on cholesterol-extracted and replenished virus. Extraction with 20 mM MβCD is fully reversible, whereas extraction with 50 mM MβCD is partially reversible. Values and error bars represent the mean and SD calculated from four to six independent experiments per condition in panel *B* and seven to 11 independent experiments per condition in panel *C*.

1:2560 for each sample in two independent experiments, indicating that hemagglutination activity was intact to within the 2-fold sensitivity of the assay (see Supporting Material). Finally, methyl-β-cyclodextrin primarily extracts sterols from lipid membranes, but related cyclodextrins can bind other lipid components (20). We performed assays of phosphate content on the cyclodextrin after extraction. At 10 and 20 mM MβCD, the phosphate content was at the limit of detection, but at 50 mM MβCD, we cannot exclude the possibility that some phospholipid was extracted from the viral membrane. It is therefore possible that the slowing of fusion at 50 mM MβCD treatment may be due to a combination of cholesterol extraction and other, minor changes to membrane composition.

The curvature effects of cholesterol are especially important for fusion because membrane fusion is believed to proceed via highly curved intermediates (21). Low levels of cholesterol impair influenza membrane fusion, as demonstrated by prior work on influenza virus or hemagglutinin-transfected cells (18,22). Similar effects have been seen in model membranes (23). The theoretical explanation for this is that cholesterol has a negative spontaneous curvature (11) and reduces the energy of highly curved fusion intermediates (24). Cholesterol can also be enriched in highly curved regions of model membranes (10). In our experiments, increasing the mole fraction of cholesterol in target liposomes increased the viral fusion rates, which agrees with hypothesis that cholesterol stabilizes the negative curvature of high-energy fusion intermediates.

Cholesterol also controls the spatial localization of viral fusion proteins, providing yet another mechanism to modulate fusion behavior. Influenza hemagglutinin localizes into cholesterol-rich regions of cellular membranes (25), and this localization is believed to be important for efficient fusion (26). Cholesterol content can affect the patterning and dynamics of viral envelopes, particularly because it alters temperature-sensitive lipid-phase behavior (27). Because multiple hemagglutinin trimers are believed to be necessary for efficient fusion (28), changes to hemagglutinin spatial patterning may alter the viral fusion kinetics. In this study, cholesterol depletion from the viral envelope produced a complex effect: moderate depletion increased the rate of fusion and severe depletion slowed it significantly. This biphasic behavior may reflect the different physical roles of cholesterol in the viral membrane. Extraction may alter hemagglutinin lateral distribution, mobility, lipid-phase behavior, and the free energies of fusion intermediates. Recent NMR spectroscopic studies on influenza virus showed the coexistence of ordered and disordered lipid domains, with a gel phase triggered by cholesterol depletion (27). Such phase changes would also alter hemagglutinin mobility.

CONCLUSIONS

Our results suggest that sterol-dependent changes to the viral envelope are multifunctional. This complexity itself is not a surprise, but it is striking that the multiple mechanistic roles of cholesterol can be seen in multiphasic fusion kinetics. Consistent with prior observations, we observed that both viral and target membrane cholesterol act to promote fusion efficiency, and depletion of either one reduces efficiency. The complex effects of cholesterol are apparent only in measurements of fusion kinetics. These effects can be deconvolved by further experiments to probe the spatial

organization and mobility of hemagglutinin in cholesterol-depleted virus. Functional assays on live virus, as presented here, are necessary to link these physical changes to viral entry kinetics.

SUPPORTING MATERIAL

Supporting material, four figures, references (29,30), and one table are available at http://www.biophysj.org/biophysj/supplemental/S0006-3495(13)00880-1.

We thank J. White, L. Tamm, C. Stroupe, and D. Steinhauer for many helpful discussions.

This work was supported by NIH R01 GM098304.

REFERENCES

1. Skehel, J. J., and D. C. Wiley. 2000. Receptor binding and membrane fusion in virus entry: the influenza hemagglutinin. *Annu. Rev. Biochem.* 69:531–569.
2. Hernandez, L. D., L. R. Hoffman, …, J. M. White. 1996. Virus-cell and cell-cell fusion. *Annu. Rev. Cell Dev. Biol.* 12:627–661.
3. Blumenthal, R., S. A. Gallo, …, A. Puri. 2002. Fluorescent lipid probes in the study of viral membrane fusion. *Chem. Phys. Lipids.* 116:39–55.
4. Kemble, G. W., T. Danieli, and J. M. White. 1994. Lipid-anchored influenza hemagglutinin promotes hemifusion, not complete fusion. *Cell.* 76:383–391.
5. Melikyan, G. B., J. M. White, and F. S. Cohen. 1995. GPI-anchored influenza hemagglutinin induces hemifusion to both red blood cell and planar bilayer membranes. *J. Cell Biol.* 131:679–691.
6. Qiao, H., R. T. Armstrong, …, J. M. White. 1999. A specific point mutant at position 1 of the influenza hemagglutinin fusion peptide displays a hemifusion phenotype. *Mol. Biol. Cell.* 10:2759–2769.
7. Munger, J., B. D. Bennett, …, J. D. Rabinowitz. 2008. Systems-level metabolic flux profiling identifies fatty acid synthesis as a target for antiviral therapy. *Nat. Biotechnol.* 26:1179–1186.
8. Aloia, R. C., H. R. Tian, and F. C. Jensen. 1993. Lipid composition and fluidity of the human immunodeficiency virus envelope and host cell plasma membranes. *Proc. Natl. Acad. Sci. USA.* 90:5181–5185.
9. Gerl, M. J., J. L. Sampaio, …, K. Simons. 2012. Quantitative analysis of the lipidomes of the influenza virus envelope and MDCK cell apical membrane. *J. Cell Biol.* 196:213–221.
10. Wang, W., L. Yang, and H. W. Huang. 2007. Evidence of cholesterol accumulated in high curvature regions: implication to the curvature elastic energy for lipid mixtures. *Biophys. J.* 92:2819–2830.
11. Chen, Z., and R. P. Rand. 1997. The influence of cholesterol on phospholipid membrane curvature and bending elasticity. *Biophys. J.* 73:267–276.
12. Simons, K., and M. J. Gerl. 2010. Revitalizing membrane rafts: new tools and insights. *Nat. Rev. Mol. Cell Biol.* 11:688–699.
13. Lingwood, D., and K. Simons. 2010. Lipid rafts as a membrane-organizing principle. *Science.* 327:46–50.
14. Hambleton, S., S. P. Steinberg, …, A. A. Gershon. 2007. Cholesterol dependence of varicella-zoster virion entry into target cells. *J. Virol.* 81:7548–7558.
15. Linetti, A., A. Fratangeli, …, P. Rosa. 2010. Cholesterol reduction impairs exocytosis of synaptic vesicles. *J. Cell Sci.* 123:595–605.
16. Rosa, P., and A. Fratangeli. 2010. Cholesterol and synaptic vesicle exocytosis. *Commun. Integr. Biol.* 3:352–353.
17. Huang, H., Y. Li, …, Y. Mori. 2006. Human herpesvirus 6 envelope cholesterol is required for virus entry. *J. Gen. Virol.* 87:277–285.
18. Sun, X., and G. R. Whittaker. 2003. Role for influenza virus envelope cholesterol in virus entry and infection. *J. Virol.* 77:12543–12551.
19. Pucadyil, T. J., and A. Chattopadhyay. 2004. Cholesterol modulates ligand binding and G-protein coupling to serotonin(1A) receptors from bovine hippocampus. *Biochim. Biophys. Acta.* 1663:188–200.
20. Zidovetzki, R., and I. Levitan. 2007. Use of cyclodextrins to manipulate plasma membrane cholesterol content: evidence, misconceptions and control strategies. *Biochim. Biophys. Acta.* 1768:1311–1324.
21. Chernomordik, L. V., and M. M. Kozlov. 2008. Mechanics of membrane fusion. *Nat. Struct. Mol. Biol.* 15:675–683.
22. Biswas, S., S. R. Yin, …, J. Zimmerberg. 2008. Cholesterol promotes hemifusion and pore widening in membrane fusion induced by influenza hemagglutinin. *J. Gen. Physiol.* 131:503–513.
23. Haque, M. E., T. J. McIntosh, and B. R. Lentz. 2001. Influence of lipid composition on physical properties and peg-mediated fusion of curved and uncurved model membrane vesicles: "nature's own" fusogenic lipid bilayer. *Biochemistry.* 40:4340–4348.
24. Kozlovsky, Y., and M. M. Kozlov. 2002. Stalk model of membrane fusion: solution of energy crisis. *Biophys. J.* 82:882–895.
25. Hess, S. T., T. J. Gould, …, J. Zimmerberg. 2007. Dynamic clustered distribution of hemagglutinin resolved at 40 nm in living cell membranes discriminates between raft theories. *Proc. Natl. Acad. Sci. USA.* 104:17370–17375.
26. Takeda, M., G. P. Leser, …, R. A. Lamb. 2003. Influenza virus hemagglutinin concentrates in lipid raft microdomains for efficient viral fusion. *Proc. Natl. Acad. Sci. USA.* 100:14610–14617.
27. Polozov, I. V., L. Bezrukov, …, J. Zimmerberg. 2008. Progressive ordering with decreasing temperature of the phospholipids of influenza virus. *Nat. Chem. Biol.* 4:248–255.
28. Danieli, T., S. L. Pelletier, …, J. M. White. 1996. Membrane fusion mediated by the influenza virus hemagglutinin requires the concerted action of at least three hemagglutinin trimers. *J. Cell Biol.* 133: 559–569.
29. Hirst, G. K. 1942. The quantitative determination of influenza virus and antibodies by means of red cell agglutination. *J. Exp. Med.* 75:49–64.
30. Bligh, E. G., and W. J. Dyer. 1959. A rapid method of total lipid extraction and purification. *Can. J. Biochem. Physiol.* 37:911–917.

Multiphasic effects of cholesterol on influenza fusion kinetics reflect multiple mechanistic roles

Marta K. Domanska,* Dominik Wrona,* and Peter M. Kasson*

*Departments of Molecular Physiology and Biological Physics and Biomedical Engineering, University of Virginia, Charlottesville, Virginia 22908, USA.

*Correspondence: kasson@virginia.edu

Supporting Information

Supplementary Materials and Methods

Materials.

Lipids: 1-Palmitoyl-2-oleoyl-*sn*-glycero-3-phosphocholine (POPC), 1-Palmitoyl-2-oleoyl-*sn*-glycero-3-phosphoethanolamine (POPE), 1,2-dioleoyl-sn-glycero-3-phospho-ethanolamine-N-(7-nitro-2-1,3-benzoxadiazol-4-yl) (NBD-DOPE), and 1,2-dioleoylsn-glycero-3-phosphoethanolamine-N-(lissamine rhodamine B sulfonyl) (ammonium salt) (Rh-DOPE) were purchased from Avanti Polar Lipids, Alabaster, AL and used without further purification.

Cholesterol, sodium chloride, sodium phosphate dibasic, sodium phosphate monobasic, citric acid, sodium hydroxide, methyl-*β*-cyclodextrin and other chemicals were purchased from Sigma, St. Louis, MO. Chloroform, ethanol, cell culture supplies (Fisher Scientific, Fair Lawn, NJ). Amplex Red Cholesterol Assay kit, ANTS and DPX were purchased from Life Technologies**,** Grand Island, NY. Purified X:31 influenza virus (A/Aichi/68 (H3N2)) was purchased from Charles River Laboratories.

Liposome preparation.

Large unilamellar vesicles (LUVs) at the specified compositions were prepared by extrusion and size exclusion chromatography as detailed below. Briefly, stock lipid solutions in chloroform were mixed in a glass test tube, dried under the argon stream and placed under vacuum for additional 1 to 2 hours. Next, the dried lipid film was hydrated with fusion buffer (FB buffer: 10 mM phosphate/90 mM citrate/150 mM NaCl, pH7.4) containing ANTS/DPX (12.5 mM ANTS/45 mM DPX) at a final lipid concentration of 2 mM. The mixture was vortexed for 5 to 10 min to form a multilamellar vesicle suspension, which was frozen and thawed five times in liquid nitrogen and a warm water bath. The multilamellar vesicle suspension was then extruded 15-20 times through two polycarbonate membranes of 100 nm pore size. In the final step, the LUVs were purified on a G50 superfine column to remove the unencapsulated ANTS and DPX. To ensure vesicle stability, osmolarity of all buffers was measured and adjusted using a cryoscopic osmometer (Osmomat 030, Gonotec).

Cholesterol determination.

The cholesterol content of influenza virus membranes was estimated using an Amplex Red Cholesterol Assay Kit according to the manufacturer's instructions. Virus was measured at 2 mg/ml. Briefly, 50 μL of 0, 10 mM, 20 mM and 50 mM MβCD treated virus and untreated virus, each containing 22 μg viral protein per sample were resuspended in Amplex Red working buffer. After a 30-60 min incubation, fluorescence was measured using excitation, emission and cutoff wavelengths of 560, 590, and 570 nm, respectively. Samples with saturating signal were re-run at 2x or 10x lower viral protein content and corrected accordingly.

Cholesterol replenishment of MβCD-treated influenza virus.

Cholesterol-depleted influenza virus was treated with previously prepared water-soluble cholesterol:MβCD complex. The complex was prepared by dissolving MβCD in 50mM Tris pH 7.5, addition of solid cholesterol and overnight vortexing. The solution was filtered to remove insoluble cholesterol crystals, and the ratio of cholesterol to MβCD was estimated (values ranged between 1.5:40 and 2:40). The virus was mixed with this complex at a 1:1 ratio, and Tris buffer

was added to obtain a final concentration of 10mM MβCD. The mixture was incubated at 37°C for 30 minutes, centrifuged at 4° C and 14000 rpm for 40 minutes, and resuspended in the fusion buffer. The kinetics of fusion between such treated virus and liposomes containing 20 mol% cholesterol were measured as described previously. The concentration of cholesterol was estimated using the Amplex Red assay.

Viral lipid extraction.

Viral lipid was extracted from the viral particles via the Bligh and Dyer extraction procedure (1). Briefly, 80 μl of virus at 2mg/ml was mixed with methanol-HCl/chloroform mixture at a 1:2:0.8 v/v/v ratio. After one hour incubation at room temperature, 100 μL of water and chloroform each were added to the mixture and spun down for 30 seconds at 14000 rpm. The organic layer was removed and transferred to a glass tube. The upper aqueous layer was re-extracted with 200 μL of chloroform and again spun down for 30 seconds at 14000 rpm. Again, the bottom layer was removed and combined with previous organic layer. Finally, the organic fraction was re-purified by back-extraction with 760 μL of chloroform/methanol-HCl/water mixture. The aqueous layer was removed by aspiration after a brief spin. The remaining organic layer containing viral lipids was dried in a speed-vac. Dried viral lipids were then used directly for phosphate analysis.

Phosphate assay.

Analysis of phospholipids were performed using a standard phosphate assay, where lipids were digested with perchloric acid and the released phosphate was reacted with ammonium molybdate in the presence of reducing agent, such as ascorbic acid, forming a blue complex. The amount of the phosphate complex was measured by absorbance at 820 nm and compared to the standard inorganic phosphate. For viral phospholipid assessment, previously extracted lipids were mixed with 10 μL of 2% ammonium molybdate, vortexed and dried in a speed-vac for 30 min. Then 300 μL of 70% perchloric acid was added to the glass tube, and the tube was heated at 180 °C for 30 min. After tube was cooled to room temp, 1.5 mL of 0.4 % ammonium molybdate and 0.22 mL of 10% (w/v) ascorbic acid were added, vortexed and heated for 10 min at 90° C. Tubes were cooled down to room temp for 20 min and absorbance at 820 nm was measured. Standard were assayed using inorganic phosphate: 0, 10, 50, 100 and 125 μL of 1mM K_2HPO_4 solution.

Hemagglutination titers.

A standard hemagglutination assay (2) was performed. Serial twofold dilutions of the virus sample were made in the PBS buffer and placed on a V-bottom plate. Next 0.5% (v/v) chicken red blood cells were added to each well at 1:1 (v:v) virus to blood cell ratio. The plate was incubated for 1 hour at 4°C. The HA titer was defined as the most diluted viral sample that formed a lattice rather than a distinct blood cell spot at the bottom of the well.

Supplementary Note

Control experiments to calculate the fraction of contents signal attributable to contents leakage were performed as follows. 100 nm liposomes were prepared with molar ratios 30:47:20:1.5:1.5 POPE:POPC:Cholesterol:NBD-DOPE:Rh-DOPE encapsulating ANTS only rather than ANTS/DPX complex. Fusion experiments with X-31 influenza virus were run on four pairs of samples with 0 and 36 mM DPX respectively in the external buffer. Fluorescence intensity values I_0, $I_{plateau}$, and I_{max} were recorded at the time of acidification, plateau value during the fusion reaction (taken as the average value over minutes 12-15), and lysis with 1% Triton X-100. The fluorescence signal due to ANTS leakage was estimated as the difference: $(I_{plateau-DPX} - I_{0-DPX}) - (I_{plateau+DPX} - I_{0+DPX}) = I_{\Delta}$. This is the fluorescence intensity increase upon fusion that is present without DPX quencher in the buffer but missing when DPX quencher is present. In the case of leakage, DPX could also leak into the liposomes, which would decrease signal. The above difference I_{Δ} is thus an upper bound on the leakage intensity when considering DPX leakage. Intensity values I_{Δ} were converted to ANTS concentration in the external compartment using an ANTS standard curve measured under the same buffer conditions. A second standard curve with ANTS and 30 mM DPX in the external compartment showed 89 ± 1 % quenching by DPX at the calculated ANTS concentration. Taking into account this quenching, the concentration of leaked ANTS in the external compartment was estimated at 420 ± 3 nM.

A standard phosphate assay yielded a phospholipid concentration of approximately 1.2 mM. Using the approximate diameter of the vesicles (110 ± 10 nm as determined by dynamic light scattering), a spherical geometry approximation, and an estimate of the area per phospholipid head group and cholesterol (tested over the range over the range 50-60 $Å^2$ per phospholipid and 12-14 $Å^2$ per cholesterol), we can estimate the vesicle contents volume at 0.10 μL in the 150 μL fusion reaction. We can then derive the approximate concentration of encapsulated ANTS to be 6.8 μM when averaged over the full reaction volume. This would correspond to 6.2% vesicle contents leakage (5.7% to 6.8% depending on the lipid area estimate). Using a series of experiments under the same conditions as above except with encapsulated ANTS/DPX and DPX in the external compartment, this level of leakage is calculated to result in a fluorescence signal of 1.18 intensity units, or 8.7 ± 0.1 % of the observed $(I_{plateau} - I_0)$ value. The remaining 91.3% of signal upon fusion is thus estimated as due to contents mixing. This estimate relies on a large number of approximations, but it suggests that the ANTS/DPX encapsulation scheme we use with DPX quencher in the buffer is largely successful at suppressing leakage signal.

Supplementary Figures

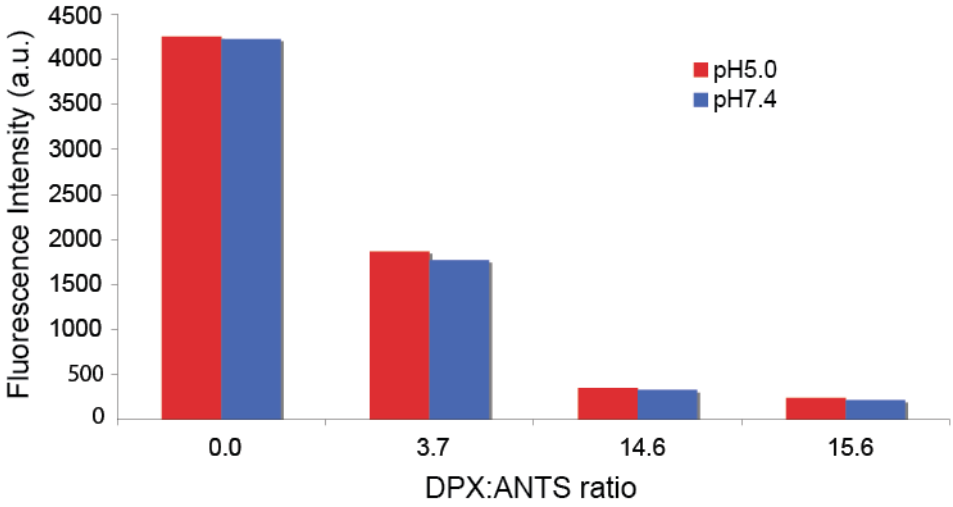

Figure S1. Solution quenching of ANTS fluorescence by DPX. ANTS fluorescence emission at 530 nm was measured for solutions containing 2.3 mM ANTS and 0, 8.6, 34, or 36 mM DPX. 2.3 mM ANTS is a loose upper bound on the final ANTS concentration were all encapsulated ANTS to leak into the reaction buffer during a fusion experiment. If full leakage occurred the final DPX concentration would be ~34 mM (14.6 DPX:ANTS ratio), resulting in >90% quenching of ANTS fluorescence. A more precise calculation (although one involving several approximations) is given in the Supplemental Note above and suggests that the actual concentration after full leakage would be closer to 7 μM.

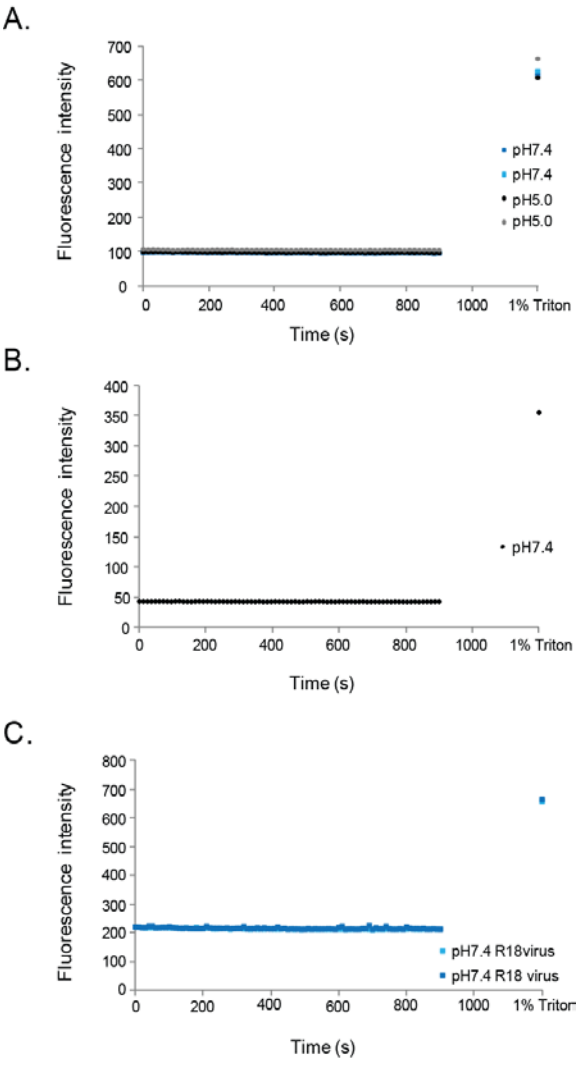

Figure S2. Labeled lipids do not detectably transfer in the absence of fusion. Plotted are a series of control experiments to test for labeled lipid transfer between pairs of 100 nm vesicles or between vesicles and X:31 influenza virus under nonfusogenic conditions. Panel **A** shows duplicate fluorescence traces for a mixture of labeled and unlabeled vesicles incubated at either pH 5.0 or pH 7.4. Vesicles containing 20 mol % cholesterol were labeled with 1.5 mol % each of NBD-DOPE and Rh-DOPE. Panel **B** shows a similar trace for labeled vesicles and unlabeled virus under the conditions used for fusion except that the pH was maintained at 7.4. Panel **C** shows a similar experiment except that unlabeled vesicles were incubated with X:31 virus that had been labeled with R18 dye. All lipid dyes were loaded at quenching concentrations; a final time point in each panel shows the fluorescence increase upon addition of 1% Triton X-100. Under none of these conditions did we observe non-fusion transfer of dye (which would manifest as an increase in fluorescence) on the time scale of our fusion experiments. R18 dye would be expected to undergo some such transfer on substantially longer timescales, however.

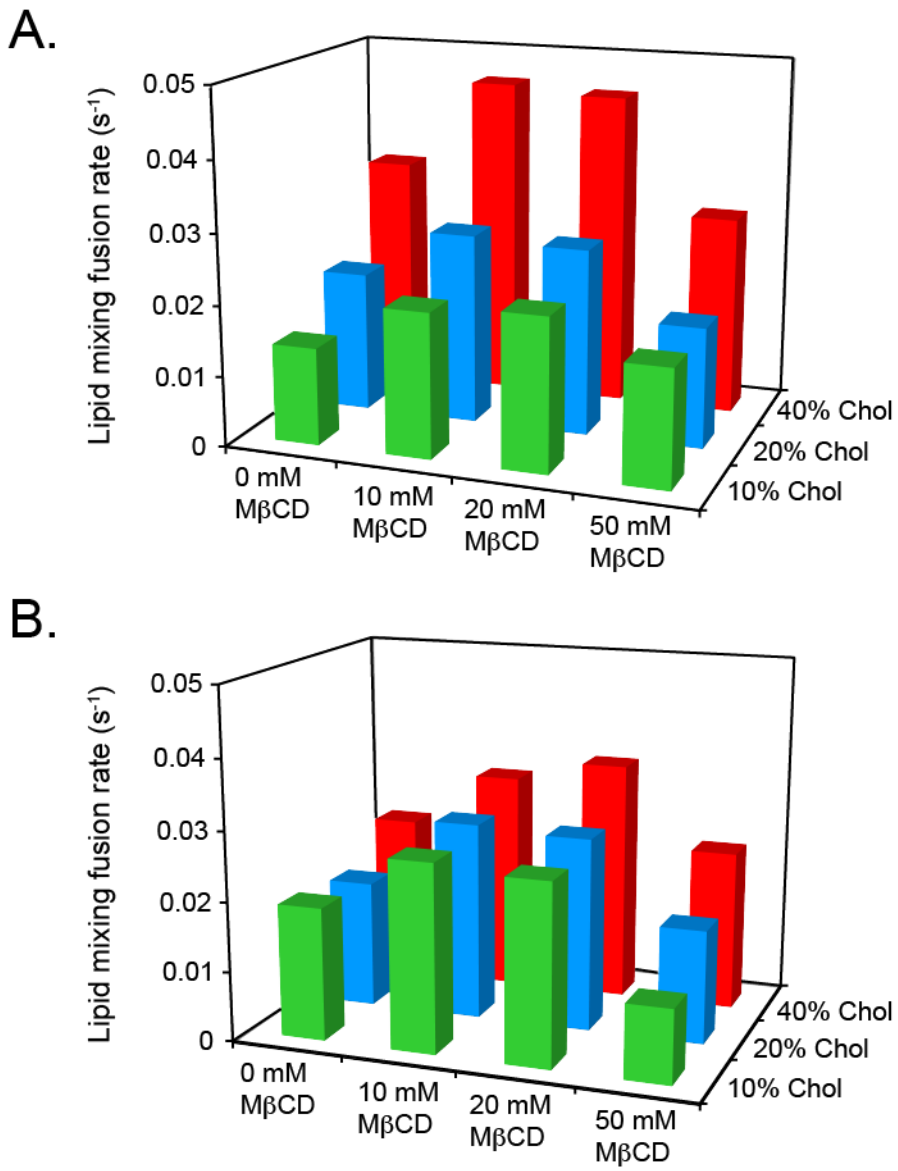

Figure S3. Fusion rates vary with cholesterol regardless of whether PC:PE ratio or PE mol % is held constant. Fusion experiments were performed either holding the mol % POPE fixed at 30% in target vesicles (panel **A**) or holding the POPC:POPE ratio fixed at 2:1 (panel **B**). The response of fusion rates to mol % cholesterol in target vesicles and to extraction of cholesterol from the virus is similar in both cases. Bars plotted represent the median of at least 3 experiments at each condition.

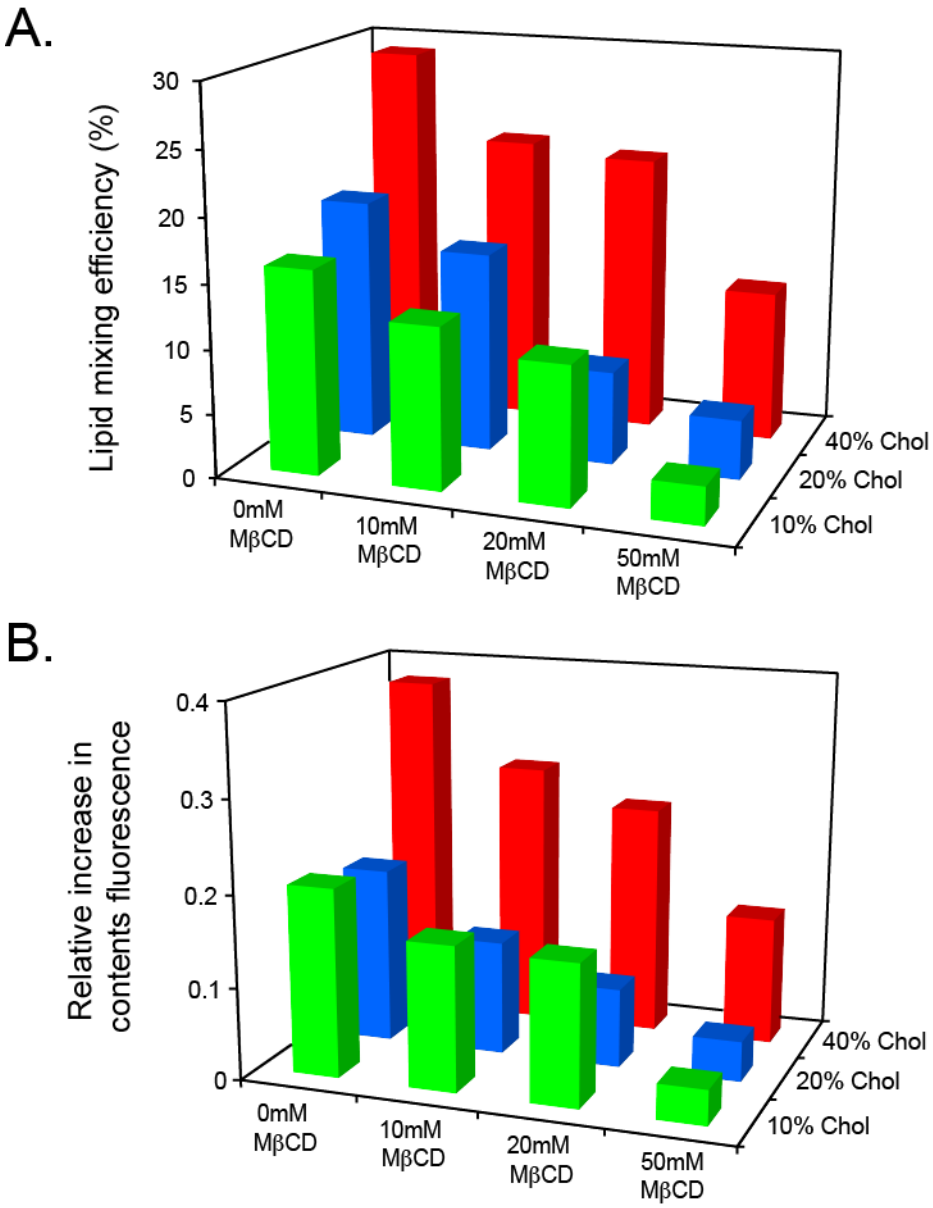

Figure S4. Extent of lipid and contents mixing shows a consistent decrease with decreasing cholesterol. Panel **A** shows lipid mixing efficiency values at each target vesicle composition and MβCD treatment tested. Panel **B** shows the extent of contents dye dequenching for the same conditions. Unlike fusion rates, efficiencies show a monotonic response to cholesterol to within error in either virus or target membrane, with lower cholesterol compositions reducing efficiency. Efficiency values were calculated from exponential fits to fluorescence dequenching traces as described in the Supporting Methods. Each bar represents the median of 5-13 independent experiments. Measurements at 10 mol % cholesterol had a larger error range, particularly for contents mixing.

Supplementary Table

Sample	ANTS fluorescence (a.u)	NBD fluorescence (a.u)
Prior to acidification	42	43
Fusion end product (15 min)	66	164
Purified vesicle fraction (normalized)	62	186
Volume-matched control, unpurified fusion end product	70	186

Table S1. Contents fluorescence in isolated vesicles after fusion..
A fusion reaction between X:31 influenza virus and 100 nm vesicles containing 20 mol % cholesterol was performed. After 15 minutes, a sample was added to a 1.2 mL Sephadex G50 spin column and spun at 4° C and 1000 x *g* for 2 minutes. The purified vesicle fraction eluted from the column was volume-matched to a control set of fusion end products that was maintained at 4° C after the 15-minute fusion reaction at 37° C rather than undergoing purification. Samples were also normalized for column yield using NBD fluorescence. The purified sample of fusion products (and unfused reactants) accounts for 86% of the fluorescence increase observed during the fusion reaction. Since this experiment did not control for vesicle leakage during purification, only lipid loss, the intra-luminal fluorescence at the end of the fusion reaction is likely even higher than this.

Supporting References.

1. Bligh, E. G., and W. J. Dyer. 1959. A rapid method of total lipid extraction and purification. Can J Biochem Physiol 37:911-917.
2. Hirst, G. K. 1942. The Quantitative Determination of Influenza Virus and Antibodies by Means of Red Cell Agglutination. J Exp Med 75:49-64.